Geochemistry Geophysics Geosystems G3
AN ELECTRONIC JOURNAL OF THE EARTH SCIENCES
Published by AGU and the Geochemical Society

Article
Volume 9, Number 12
9 December 2008
Q12X03, doi:10.1029/2008GC002186
ISSN: 1525-2027

Click Here for Full Article

Earthquake evidence for along-arc extension in the Mariana Islands

David S. Heeszel, Douglas A. Wiens, and Patrick J. Shore
Earth and Planetary Sciences, Washington University, Campus Box 1169, 1 Brookings Drive, St. Louis, Missouri 63130, USA (davidh@seismo.wustl.edu)

Hajime Shiobara
Earthquake Research Institute, University of Tokyo, Tokyo 113-0032, Japan

Hiroko Sugioka
IFREE, JAMSTEC, Yokosuka 237-0061, Japan

[1] Analysis of data from a deployment of ocean bottom and land seismographs in 2003–2004 detected four swarms of earthquakes in the overriding plate of the Mariana subduction system between the fore-arc and the back-arc spreading center. Two additional shallow swarms were identified by analyzing the teleseismic earthquake catalogs from 1967 to 2003. Focal mechanism solutions for these swarms, determined from regional waveform inversion for the 2003–2004 events or retrieved from the Centroid Moment Tensor catalog for previous years, suggest a complex system of deformation throughout the arc. We observe arc-parallel extension near volcanic cross chains, arc-perpendicular extension along the frontal arc, and arc-parallel compression farther into the back arc near the Mariana Trough. A swarm beneath the middle and eastern summits of the Diamante cross chain may have recorded magmatic activity. Volcanic cross chains showing evidence of adiabatic decompression melting from extensional upwelling are localized at regions of enhanced along-strike extension. The earthquake data are consistent with recent GPS results indicating 12 mm/a of extension between Guam and Agrihan. The along-arc extension may result from either increasing curvature of the Mariana system with time or from deformation induced by oblique subduction in the northernmost and southernmost regions of the arc.

Components: 6057 words, 6 figures, 2 tables.

Keywords: Mariana Islands; cross-chain volcanism; arc-parallel extension; crustal deformation; subduction zone tectonics.

Index Terms: 7240 Seismology: Subduction zones (1207, 1219, 1240); 8185 Tectonophysics: Volcanic arcs; 7230 Seismology: Seismicity and tectonics (1207, 1217, 1240, 1242).

Received 24 July 2008; **Revised** 15 October 2008; **Accepted** 22 October 2008; **Published** 9 December 2008.

Heeszel, D. S., D. A. Wiens, P. J. Shore, H. Shiobara, and H. Sugioka (2008), Earthquake evidence for along-arc extension in the Mariana Islands, *Geochem. Geophys. Geosyst.*, *9*, Q12X03, doi:10.1029/2008GC002186.

Theme: Izu-Bonin-Mariana Subduction System: A Comprehensive Overview
Guest Editors: Shuichi Kodaira, Sara Pozgay, and Jeffery Ryan

Copyright 2008 by the American Geophysical Union

1. Introduction

[2] It is widely understood that the geometry of island arcs must change as the configuration of the trench and the downgoing slab evolves. Tectonic reconstructions have documented large changes of arc curvature for several subduction zones in the geologic record [*Barker and Dalziel*, 1983; *Hall et al.*, 1995]. Geodynamic modeling studies have shown that slabs with limited along-strike length (<1500 km) tend to develop strong curvature due to the retreat of the slab edges [*Schellart*, 2005; *Schellart et al.*, 2007]. Changes in slab geometry and curvature must cause significant deformation of the overriding plate, but actual documentation of ongoing deformation and its possible links to volcanic and other tectonic processes in present-day arcs has been limited.

[3] The Mariana Arc presents an ideal opportunity to study the deformation of the overriding arc microplate and associated effects on volcanism in response to changes in slab geometry. The currently active Mariana Arc developed at approximately 7 Ma [*Stern et al.*, 2003] because of the formation of the Mariana Trough and the migration of arc volcanism from the previous arc (currently the west Mariana Ridge) to the currently active volcanic arc. The curvature of the Mariana Arc has increased through time as can be seen in maps of the Philippine Sea basin in which the original arc, the Palau Kyushu ridge (see Figure 1 inset), is nearly straight. Subsequent arcs, the West Mariana Ridge and the active Mariana Arc, indicate increasing curvature with time (see *Stern et al.* [2003] for a review). The Mariana Trough has a spreading rate that changes along the length of the arc, decreasing from 45 mm/a in the south near Guam to 15 mm/a in the north [*Kato et al.*, 2003] and eventually transitions from seafloor spreading to rifting north of 20°N [*Martinez et al.*, 2000]. Additionally, the relative subduction direction changes over the length of the arc. It is trench-perpendicular through the central region of the arc and increases in obliquity to the north and the south [*Bird*, 2003]. Evidence for arc-parallel extension in the Mariana microplate also exists in the form of numerous serpentinite seamounts in the fore arc, some of which are upthrown horsts [*Fryer*, 1996] and bathymetric mapping data that indicates a large number of roughly trench-perpendicular normal faults in the Mariana fore arc [*Stern and Smoot*, 1998]. Geodetic results also indicate significant arc-parallel extensional strains in the Mariana Arc [*McCaffrey*, 1996; *Bird*, 2003; *Kato et al.*, 2003].

[4] Volcanic cross chains occur throughout the Mariana Arc and are apparent in bathymetric images as a line of high structures extending from the active arc into the back arc (Figure 1). Several have had their geochemistry studied in detail, particularly the cross chain extending west from Guguan Island [*Stern et al.*, 2006], a small network of cross-chain volcanoes at 14°40′N which Chaife [*Kohut et al.*, 2006] and Northwest-Rota-1 [*Embley et al.*, 2006] seamounts are a part, and the Kasuga cross chain [*Stern et al.*, 1993, *Fryer et al.*, 1997]. The chain at Guguan is morphologically typical of other cross chains in the Marianas, consisting of a large volcano at the magmatic front with one or more smaller volcanoes extending into the back arc. Geochemistry at Guguan is consistent with other arc volcanoes, but there is a decrease in the subduction component as the volcanoes extend into the back arc [*Stern et al.*, 2006]. The cross chain at 14°40′N is atypical of the other cross chains in the Mariana Arc, as it is composed of several small (mean volume of ~27 km^3) seamounts extending from the arc to the back arc in a diffuse line. Chaife seamount has been studied in detail and has an anomalous geochemistry. It is more consistent with MORB than typical arc magmas, having an Mg # of ~76, much higher than typical arc volcanism [*Kohut et al.*, 2006].

[5] The frontal arc, a region of uplifted basement rock trenchward of the volcanic front including the largest islands in the Mariana system, is also undergoing deformation [*Fryer*, 1996; *Stern et al.*, 2003]. Interpreted as an upthrown block bound on both sides by normal faults [*Stern and Smoot*, 1998], *Gvirtzman and Stern* [2004] propose that this uplift is due to a narrower plate coupling zone in the southern portion of the Mariana Arc. This narrower zone of slab "pull-down" allows the fore arc of the overriding plate to rise higher than for the more widely coupled subduction zone in the central portion of the Mariana Arc.

[6] In this paper we present the results of a 2003–2004 Mariana passive seismic experiment as well as teleseismic catalogs that recorded significant seismicity in the overriding plate, placing constraints on the present-day deformation of the Mariana platelet in response to changing slab geometry. We discuss the relationship of this seismicity and deformation to volcanic cross chains and propose that the locations of cross-chain volcanoes may be linked to localization of extensional strain. We also note several swarms of seismicity that likely are associated with previously undocumented submarine volcanic activity.

2. Data

[7] The Mariana Subduction Factory Imaging Project deployed 20 broadband land seismographs and

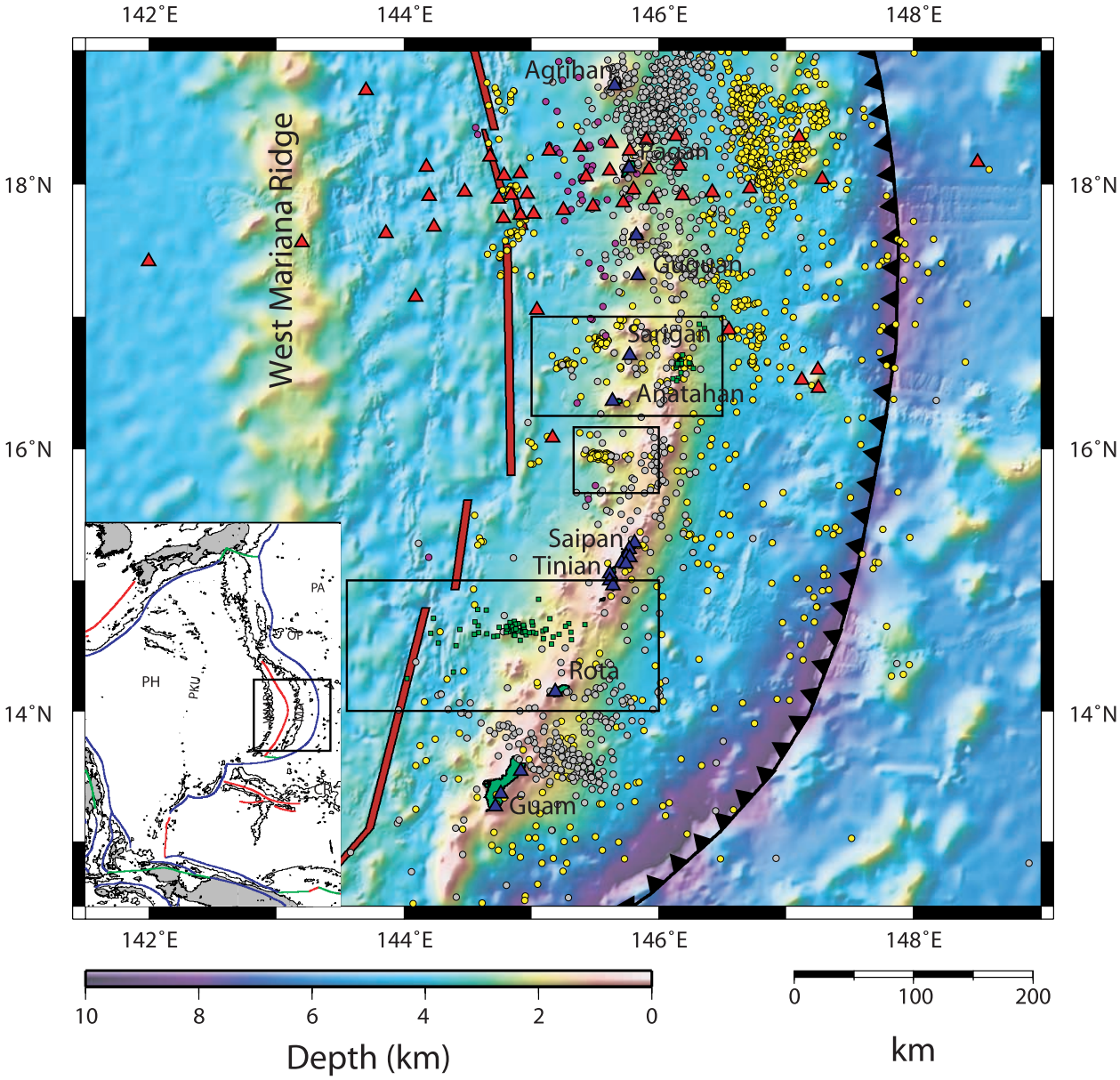

Figure 1. Bathymetric map of the Mariana Islands with stations marked as red and blue triangles (OBS and land stations, respectively). Thick red line is spreading axis of the Mariana Trough and the thick, toothed black line marks trench location with teeth toward the overriding Mariana microplate. Shallow (0–70 km), intermediate (70–300 km), and deep (>300 km) earthquakes are plotted as yellow, gray, and purple circles, respectively. Only the 2194 best located earthquakes (those with more than 10 local arrivals and semimajor error axes of less than 5 km) are plotted here. Green squares represent teleseismically detected earthquake swarms that predate the deployment and are discussed in this paper. Black boxes denote regions mapped in other figures. Inset shows regional map with black box around area of detail. Blue lines indicate trenches, red lines indicate ridges, and green lines indicate transform boundaries. The 2500 m isobath is plotted to delineate major bathymetric highs. PA: Pacific Plate, PH: Philippine Plate, MA: Mariana Arc, WMR: West Mariana Ridge, PKU: Palau-Kyushu Ridge, OP: Ogasawara Plateau, CR: Caroline Ridge.

58 semibroadband ocean bottom seismographs (OBSs) during May–June of 2003 and recovered them in April–May 2004. The land stations consisted of either Streckheisen STS-2 or Guralp 40-T seismometers and Reftek 72A-08 data loggers with GPS timing located on 10 islands between Guam and Agrihan. Each island with a station had at least one STS-2 seismograph; the 40T seismographs were deployed in denser arrays on Saipan, Tinian, and Guam. The 58 OBSs were located around the

region of deepest earthquake activity near Pagan Island extending from the forearc through the back-arc spreading center to the west Mariana Ridge (Figure 1). Lamont-Doherty Earth Observatory operated 50 OBSs that used three-component Mark Products L4 sensors with a 1-Hz natural period and modified amplifiers to extend long-period performance [*Webb et al.*, 2001]. Fifteen of these OBSs were an older 16-bit model and 35 were of a new 24-bit design. The remaining OBSs used Precision Measuring Devices (PMD-WB2023LP) sensors and were built by H. Shiobara at the University of Tokyo. The 35 new U.S. OBSs stopped recording ~50 days after deployment due to a firmware error, eight U.S. OBSs were not recovered (not plotted in Figure 1), and several U.S. OBSs failed to deploy the sensor to the seafloor properly. All of the land stations operated properly throughout the deployment with the exception of Anatahan Island, which experienced several power failures due to ash from volcanic activity [*Pozgay et al.*, 2005]. The coordinates of all stations and recovered OBSs are given by *Pozgay et al.* [2007].

3. Analysis

3.1. Earthquake Locations

[8] Earthquakes were initially detected and located using Boulder Real Time Technology's Antelope data management package [*Quinlan et al.*, 1996]. The short-term average/long-term average (STA/LTA) automatic picking routine was used to identify earthquakes and their initial locations were calculated using a grid search routine with the IASPEI91 velocity model [*Kennett and Engdahl*, 1991] used to calculate traveltimes. Subsequently, over 3400 earthquakes with a significant number of arrivals were reviewed and relocated using the GENLOC least squares location module [*Pavlis et al.*, 2004], and the best located earthquakes are plotted in Figure 1. Since IASPEI91 is a global velocity model, we relocated the closely clustered local events for this study using a one-dimensional *P* wave model of the Mariana Arc [*Takahashi et al.*, 2007] for the crust. The *S* wave model was derived from the *P* wave model using *Vp*/*Vs* ratios consistent with the crust [*Shaw*, 1994] and upper mantle [*Christensen*, 1996] of a volcanic arc. The upper mantle was modeled as PREM [*Dziewonski and Anderson*, 1981] with both the *P* and *S* wave velocities reduced by 2–5% based on modeling events of known focal mechanisms in both Tonga-Fiji and the Marianas. Most of the relocated events used in this study and the stations that detected them are either on or very near the volcanic arc, so a single velocity model was appropriate to improve the traveltime misfit.

[9] In order to further improve earthquake locations for the four observed swarms, we applied a multiple-event relative relocation program based on the hypocentroidal decomposition algorithm [*Jordan and Sverdrup*, 1981] that was modified to use the local traveltime calculator from the HYPOELLIPSE program [*Lahr*, 1999]. The program was applied to each swarm individually and only events with greater than 10 total arrivals and more than three *S* wave arrivals were included in the relocation.

[10] In addition to the four swarms detected during the 2003–2004 deployment, two previous teleseismically detected swarms were discovered in the International Seismological Center (ISC) database (http://www.isc.ac.uk). One occurred during 1990 and was located in the same region as the swarm in the fore arc observed during the 2003–2004 experiment. The second historical swarm occurred during 1997 at approximately 14°40′N, a region of anomalous volcanism. Both swarms were relocated using teleseismic *P* wave arrival times using the method of *Jordan and Sverdrup* [1981] and the IASPEI91velocity model [*Kennett and Engdahl*, 1991].

3.2. Focal Mechanisms

[11] Although the swarm earthquakes were quite small we were able to calculate focal mechanisms for seven events (Table 1), six in the swarm on the Diamante seamount chain and one in the region between west Sarigan seamount and the Mariana Trough, using regional waveform inversion. There is low signal-to-noise ratio above 0.1 Hz and significant uncertainty in the small-scale seismic velocity structure to which higher-frequency signal is sensitive. As a result, the inversions were calculated at frequencies of 0.03–0.06 Hz, a low-frequency range that has a higher signal-to-noise ratio and for which uncertainties in velocity structure are less important.

[12] To calculate focal mechanisms, we first used a reflectivity code [*Kennett*, 1983] that incorporates a water layer to calculate synthetic seismograms for three fundamental focal mechanisms. Synthetics can then be calculated for an arbitrary focal mechanism using a linear combination of these fundamental synthetics [*Langston and Helmberger*, 1975]. We use a grid search over fault strike, dip, slip, and time function duration to determine the

Table 1. Earthquake Source Parameters Determined by Regional Waveform Inversion

Event[a]	Date (mm/dd/yyyy)	Origin Time[b]	Latitude	Longitude	Depth[b] (km)	Strike	Dip	Slip	M_w
6250316	6/25/2003	1655:27	15.97	145.55	22	112	88	−61	3.73
6250322	6/25/2003	2231:33	15.97	145.55	24	78	74	−27	3.49
7110300	7/11/2003	0011:04	15.95	145.59	13	90	78	−18	3.72
8090313	8/9/2003	1345:54	16.63	145.28	25	94	32	151	4.28
8130322	8/13/2003	2253:09	15.95	145.55	21	0	48	−4	3.39
8170312	8/17/2003	1240:08	15.97	145.55	18	75	77	−53	3.29

[a] Event ID corresponds to labels in Figures 3–5.
[b] Origin time and depth determined by relocation and fixed in waveform inversion.

proper focal mechanism and seismic moment with the lowest least squares misfit for the vertical and, where there is a good signal-to-noise ratio, the transverse components. Each grid search was run 100 times with random start, step size, and number of steps to ensure the solution is not biased by the discretization of the grid search. A test focal mechanism was calculated for an earthquake in the CMT catalog near Northwest Rota that occurred close to the end of the deployment to ensure that our method accurately calculated the focal mechanisms of interest. Our results are nearly identical to those in the CMT (Figure 2).

4. Results

4.1. The 14°40′N, Northwest Rota

[13] One of the largest swarms, both in earthquake magnitude and in the number of events, occurred

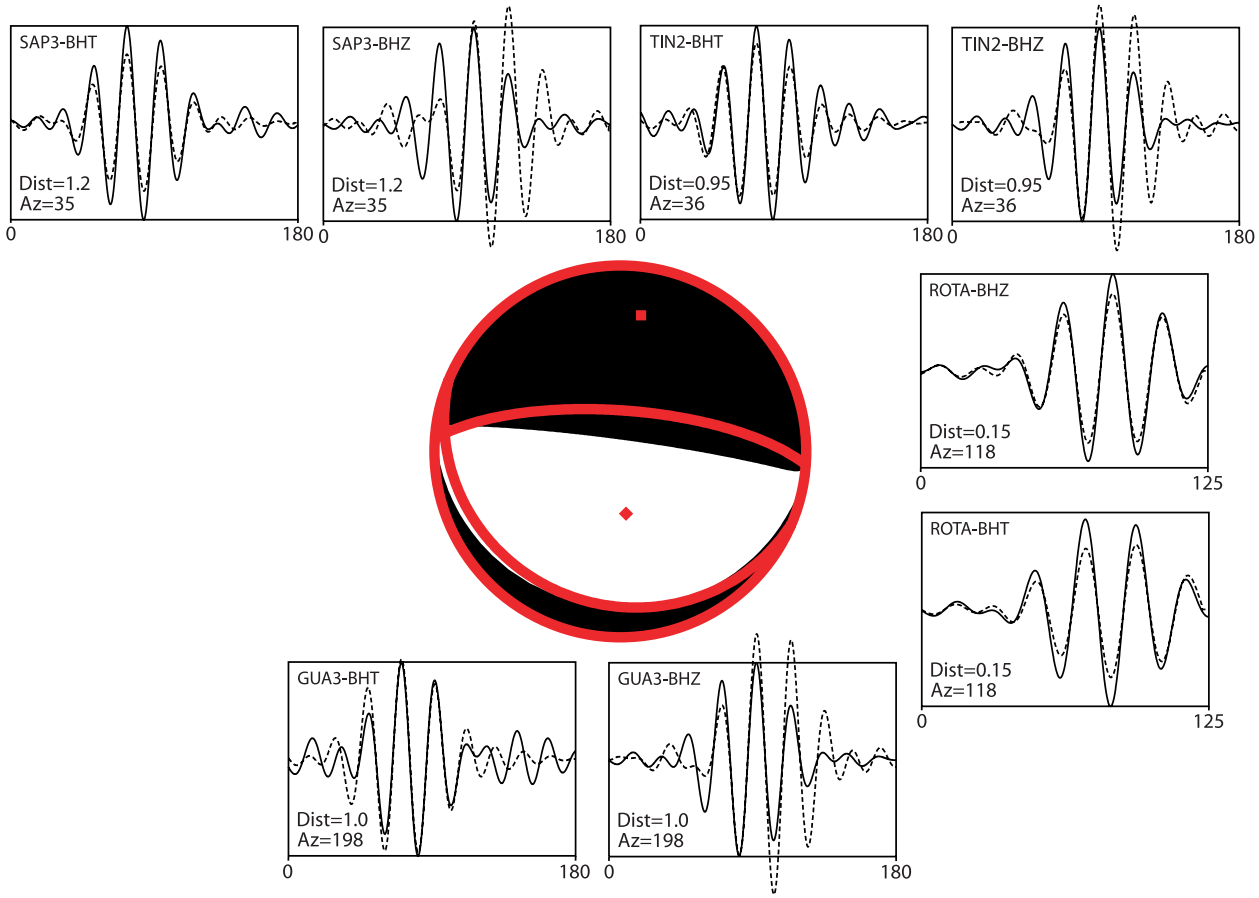

Figure 2. Example focal mechanism (red), in this case for test earthquake near northwest Rota seamount plotted over CMT solution (black). P and T axes are denoted by the red diamond and square, respectively. Waveforms plotted near their respective positions with regard to the earthquake epicenter with event station distance and azimuth given in degrees. Solid line is data and dashed is synthetic; time on x axis.

Table 2. Swarm Information

Swarm Description	Number of Earthquakes	Mean Latitude	Mean Longitude	Mean Depth	Mean 2σ Depth Uncertainty (km)	Mean Magnitude	Minimum Magnitude	Maximum Magnitude	Start Date (mm/dd/yyyy)	End Date (mm/dd/yyyy)
14°40′N/Northwest Rota	64	14.62	144.91	31.1	fixed in inversion[a]	4.12[b]	3.70[b]	4.90[b]	8/29/1997	10/9/1997
Diamante	111	15.96	145.55	17.4	2.4	3.20[c]	2.81[c]	4.12[c]	6/22/2003	9/5/2003
Northwest Sarigan	33	16.84	145.56	23.2	2.2	3.13[c]	2.71[c]	3.81[c]	12/15/2003	1/14/2004
16°40′N/Mariana Trough	21	16.63	145.28	23.7	2.2	3.41[c]	2.59[c]	4.31[c]	7/4/2003	9/11/2003
Fore arc Teleseismic	13	16.55	145.98	28.5	fixed in inversion[a]	4.75[b]	4.30[b]	5.30[b]	3/29/1990	4/29/1990
Fore arc Local	19	16.65	146.14	19.6	3.3	3.12[c]	2.64[c]	3.53[c]	10/1/2003	1/10/2004

[a] Owing to poor depth constraint from teleseismic *P* wave arrivals, earthquake depths are fixed for relative relocations of teleseismic swarms.
[b] M_b is from International Seismological Center database.
[c] M_{local} is from Antelope database.

on an E–W trending line from just northwest of Rota Island to the Mariana Trough at a latitude of approximately 14°40′N. This swarm of 64 events occurred in August and September of 1997 (see Table 2 for details). Nearly two thirds of the earthquakes in the swarm occurred during a 2-day period (29–30) in August, though there was no large main shock to indicate that this is an aftershock sequence. We used teleseismic arrival times from the ISC to relocate these events using the hypocentroidal decomposition method. A few of the westernmost events lie on the Mariana Trough, but the majority are located on or very near a diffuse, E–W trending line of small volcanic seamounts running perpendicular to the volcanic arc (Figure 3) from the magmatic front to the back-arc spreading center. Geochemical analysis of two seamounts in this cross-chain indicate that in addition to arc style volcanism [*Embley et al.*, 2006] adiabatic decompression melting also occurs [*Kohut et al.*, 2006]. Additionally, two of these events have solutions in the CMT database that indicate N–S extension and are plotted in their relocated positions in Figure 3. Additional CMT solutions for the area also indicate an N–S oriented extensional axis, though the westernmost solutions with E–W normal faulting are likely associated with back-arc basin tectonics.

4.2. Diamante Seamount Chain

[14] The swarm on the Diamante seamount chain (Figure 4) occurred between June and August 2003 and consisted of 111 earthquakes with depths of less than 40 km (Table 2 for average locations). None of the earthquakes associated with the swarm were detected teleseismically. We obtained focal mechanisms for six events using waveform inversion, with moment magnitudes ranging from M_w 3.3 to 3.7 (Table 1). All events share a generally E–W striking, steeply dipping fault plane and a dominantly N–S oriented tensional axis. These factors combined suggest the presence of significant N–S extension in the region of the Diamante seamount chain associated with tectonism and magmatism. Bathymetric mapping of the seamount chain also indicate strong N–S extension (Figure 4) particularly on the summit of east Diamante where the caldera is elongated in an E–W direction and contains E–W striking normal faults.

[15] The occurrence of 99 of the 111 events during a 4 week period in August 2003 and the absence of a clear main shock may indicate that this swarm is associated with active magmatism beneath one or

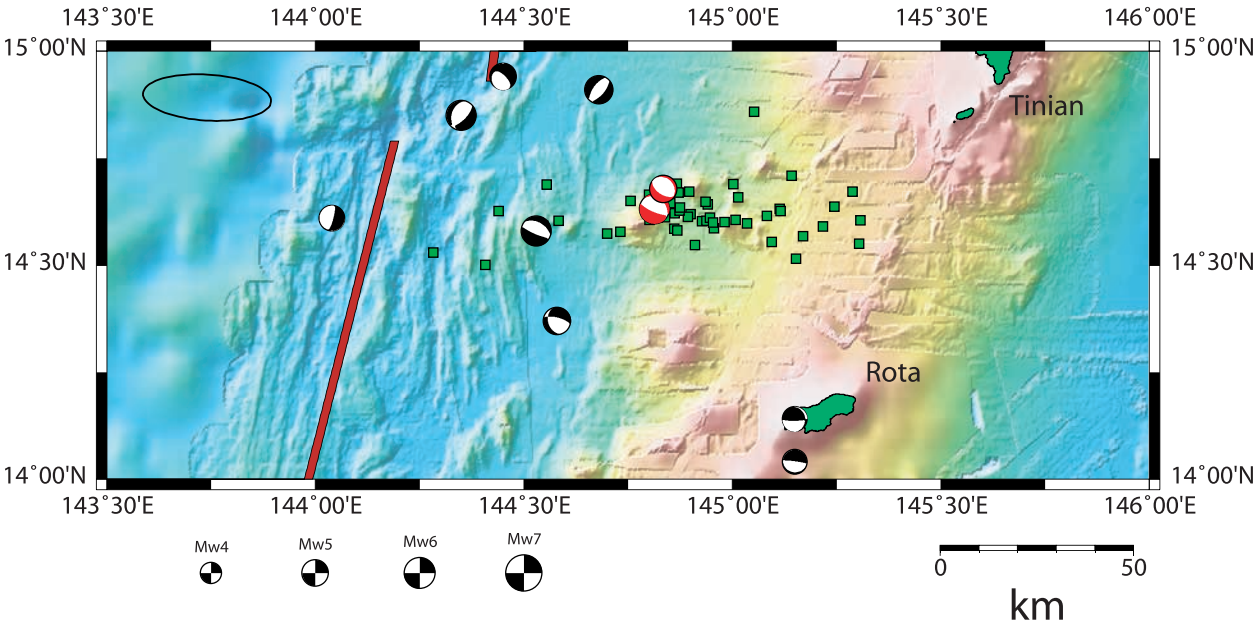

Figure 3. Shallow seismicity of the northwest Rota region during the 1997 swarm. Events extending from the uplifted arc to the back-arc spreading center indicate an extensive region of deformation due to arc-parallel stresses. CMT solutions for the region also indicated N–S extension. Green squares are relocated earthquakes, red CMTs are solutions for relocated events that occurred during the 1997 swarm, and black CMTs are other historical seismicity in the region that did not occur during the swarm and have not been relocated. Average 95% confidence ellipse plotted in upper left-hand corner. Owing to poor earthquake depth resolution for shallow earthquakes located with teleseismic arrival times, the depths of the earthquakes are poorly constrained and are therefore not plotted. Bathymetry color scale is the same as for Figure 1.

multiple volcanoes in the chain. However, earthquake locations do not indicate a progression either laterally or with depth, and the focal mechanisms, representing the largest earthquakes in the swarm, show no preferred progression in location with time. 95% confidence ellipses for this swarm average 9.2 km in a nearly east–west line, making it difficult to determine which of the seamounts the earthquakes occurred beneath, though the best located events indicate that both east Diamante and middle Diamante were seismically active. The earthquakes are spread out in a diffuse cloud that underlies both middle Diamante and east Diamante seamounts. We conclude that the swarm could indicate an eruptive event at either middle or east Diamante, or it could have resulted from magmatic activity at deeper levels beneath the seamounts.

4.3. The 16°40′N, Mariana Trough

[16] The swarm located furthest to the west, between Sarigan Island and the Mariana Trough consisted of 21 events between July and September 2003 with activity peaking during the second week of August. The earthquakes had an average depth of ~24 km, and this swarm is the only one, other than that at Diamante, for which a focal mechanism was determined from regional waveforms. This event has a focal mechanism consistent with thrust faulting with a strike-slip component and a shallowly dipping plane with a strike that is roughly parallel to a small bathymetric ridge to the west of the swarm (circled feature in Figure 5). Additionally, the rest of the swarm lies along strike with this bathymetric feature, and there is little to no bathymetric relief in the region immediately surrounding the location of the observed swarm, presumably due to sediment cover. The 95% confidence ellipses for the earthquakes are on average ~5 km in the E–W direction and smaller in the N–S, so it is unlikely that they are actually located on the bathymetric high to the west or further to the east near the volcanic arc. We suggest that this swarm is associated with compressional tectonics associated with the tectonically uplifted compression ridge in this region.

4.4. West Sarigan Seamount

[17] The earthquake swarm just northwest of West Sarigan seamount consisted of 33 events at an

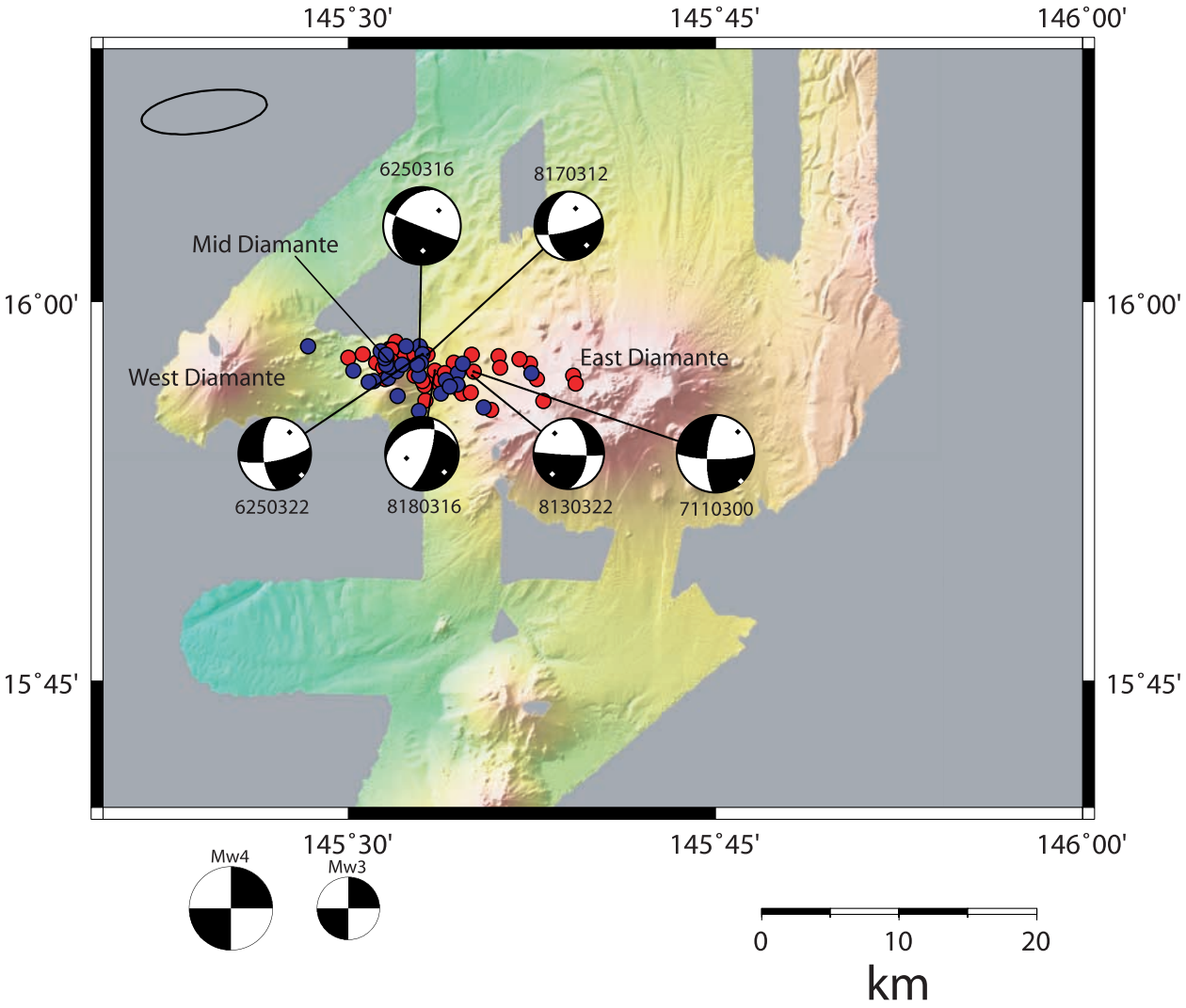

Figure 4. Detail of Diamante cross-chain area with focal mechanisms and earthquakes shown as red and blue circles representing earthquakes that are <20 km and >20 km deep, respectively. East Diamante, middle Diamante, and west Diamante seamounts are labeled. There is an E–W trending line of events centered over middle Diamante seamount. The focal mechanisms are largely consistent with an N–S extensional axis. Most share a steeply dipping E–W fault plane. Black and white diamonds on focal mechanisms represent compressional and tensional axes, respectively. Average 95% confidence ellipse plotted in upper left-hand corner. Bathymetry color scale is the same as for Figure 1. (Bathymetry courtesy of Robert Embley.)

average depth of ~17 km during December 2003 and January 2004. The absence of a main shock and the short duration of the swarm over a period of approximately 40 days (see Table 2) indicates that the swarm is likely associated with magmatic or tectonic processes very near West Sarigan seamount. The observed earthquakes are well constrained in depth by the presence of the Sarigan Island station ~25 km away. Additionally, a CMT solution from August, 2005 indicates the presence of N–S extensional faulting in the same area as the observed swarm. We interpret this swarm as the result of either north–south extension along the Sarigan volcanic cross chain or else magmatic activity near West Sarigan seamount.

4.5. Fore-Arc Rise

[18] The final two swarms are located in the fore-arc rise. One was observed by the local seismograph array and consisted of 19 earthquakes beginning in October 2003 and continuing into January 2004. They have an average depth of 27 km, consistent with the teleseismic swarm in

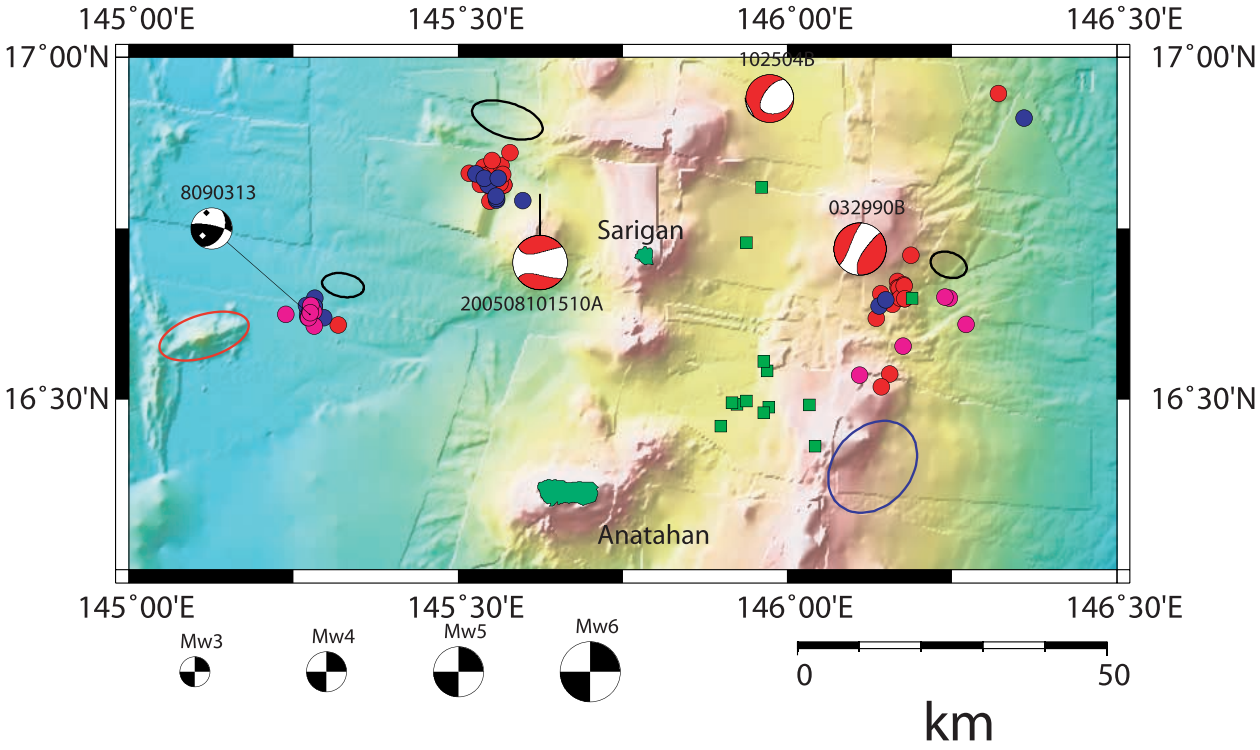

Figure 5. Region of Anatahan and Sarigan Islands where four swarms occurred. Earthquakes associated with the three locally detected earthquake swarms are shown as red (0–20 km), blue (20–30 km) and magenta (30–40 km) circles with average 95% confidence ellipses plotted in black near each swarm. The teleseismically detected earthquakes that predate (1990) our deployment are plotted as green squares with an average 95% confidence ellipse plotted in blue. The swarm at 16°40N is the only one, besides that at Diamante, for which a focal mechanism was determined. Its proximity to a small anomalous seafloor structure (red circled region) indicates potential contraction of the region between the arc and back-arc spreading center. The swarm near northwest Sarigan along with a CMT solution for the same region suggests possible volcanic activity. The two swarms in the fore arc, of which the 1990 swarm is the most spread out, are likely the result of arc-perpendicular stresses in the fore arc. Focal mechanism from this study is in black and those in red are from CMT catalog. Bathymetry color scale is the same as for Figure 1.

the same region. The teleseismic swarm occurred during March and April 1990 and consisted of 13 events at an average depth of ~28 km. The majority of events (nine) occurred during the last 3 days of March. These swarms are too far east to be of volcanic origin as there is no confirmed volcanism in the uplifted fore arc [*Fryer*, 1996; *Stern et al.*, 2003]. Additionally, the earthquakes are too far west of the trench to be associated with the shallow thrust zone. Both swarms are well located laterally, though the locally detected swarm is the most poorly constrained of the locally detected swarms due to its occurrence later in the deployment when many of the OBSs had already failed. This swarm is likely due to continued uplift of the fore arc basement material that composes the islands further to the south that *Gvirtzman and Stern* [2004] suggest is due to weak plate coupling between the subducting Pacific plate and the overriding Mariana microplate.

5. Discussion

5.1. Extensional Swarms Associated With Volcanic Cross Chains

[19] Arc-parallel extension has been documented in the southern Marianas by GPS data. GPS surveys from 1992 to 1999 [*Kato et al.*, 2003] indicate a separation rate of approximately 5 mm/a between Saipan and Guam, the closest islands for which there are results. Data from more islands, particularly Rota and Tinian, is required to discern whether this extension is localized at 14°40′N or if it is associated with a more diffuse zone of deformation. Geochemical evidence in the from Chaife

seamount a small seamount with an Mg # ~76 [*Kohut et al.*, 2006], and the seismic results presented here serve as a strong indication that the deformation is in fact concentrated at 14°40′N. *Miller et al.* [2006] proposed a slab tear in the region of 14°40′N though based on the GPS results of *Kato et al.* [2003] and the amount of intervening mantle between the downgoing slab and the overriding plate in this region we believe it is unlikely to be a significant contributor to the observed volcano-tectonic activity observed in this location. This concentration of seismicity at volcanic cross chains occurs in other locations within the Mariana Arc such as at the Diamante seamount chain indicating that the location of cross-chain volcanism is controlled by the concentration of along arc extensional stresses throughout the arc.

[20] The Diamante cross-chain volcanoes are morphologically different from those of the northwest Rota region. They are larger and fewer in number and are more consistent with those described as typical cross-chain volcanoes [*Kohut et al.*, 2006]. However, the high level of seismicity in the region coupled with the focal mechanisms determined in this study is suggestive of a similar mechanism for their formation as those to the south. The same arc-parallel extension that may control extensional volcanism to the south near 14°40′N may also play a role in the development of other, larger cross chains such as that at Diamante. Though not fully resolved, GPS results from *Kato et al.* [2003] indicate that there is approximately 3 mm/a of separation between Saipan and Anatahan which are the islands directly to the south and north of the Diamante cross chain, respectively. This suggests that the focusing of arc-parallel stresses likely controls the location of the Diamante cross chain. Additionally, the size and structure of the seamounts may be controlled by their location in the main portion of the arc rather than in the southern seamount province [*Stern et al.*, 2003] where volcanoes are typically smaller and none is of significant enough size to breach the surface.

[21] Geochemical evidence from the Guguan [*Stern et al.*, 2006] cross chain indicates that the material erupted behind the island arc becomes progressively more consistent with primitive mantle melts altered by subduction components than with typical arc magmas seen at the magmatic front (island arc) moving toward the back-arc spreading center. Data from the 14°40′N cross chain [*Kohut et al.*, 2006] indicates adiabatic decompression melting which is consistent with extensional stresses. The localization of seismic activity and a style of volcanism that is both more primitive and more indicative of passive upwelling due to extension rather than flux melting from a downgoing slab suggests that the location of cross-chain volcanism is controlled more by localization of arc-parallel extensional stress and less by subduction processes.

5.2. Seismicity and Deformation in the Mariana Microplate

[22] The observed pattern of along-strike extension in the fore arc and arc and compression near the back-arc spreading center is likely due to tectonic forces that are increasing the curvature of the Mariana microplate. The microplate is bounded on the east and south by the Mariana Trench, on the west by the Mariana Trough and associated spreading center that effectively decouples stresses in the microplate from those in the Philippine Sea plate [*Martinez et al.*, 2000], and on the north by a complex system of rifting and transform faulting [*Bird*, 2003]. Increasing curvature with the endpoints fixed will lead to along-arc extension in most of the arc and particularly on the convex side, with the possibility of compression on the concave side. In addition to the increasing curvature in the arc, the Mariana microplate is associated with the oblique subduction of the Pacific plate in the northern and southern parts of the fore arc. Oblique subduction causes sliver motion of the arc and fore arc similar to that suggested for arc-parallel extension in the Okinawa Trough [*Kubo and Fukuyama*, 2003]. This may have an additive effect in stretching the arc in the N–S direction, producing the extensional stresses resulting in cross-chain volcanoes in the arc.

[23] If the curvature of the arc is increasing then the western portion of the arc microplate will have to be undergoing compression, as indicated by the swarm and tectonically uplifted compression ridge between Sarigan Island and the back-arc spreading center. The fact that compression in the back arc is observed in only one place relatively near the spreading center may indicate that there are several regions of extensional stress due to the combined effects of increasing curvature and oblique subduction with small regions of along-arc contraction near the spreading center. The detailed along-strike distribution of extensional and compressional strain in the arc and back arc may be rather

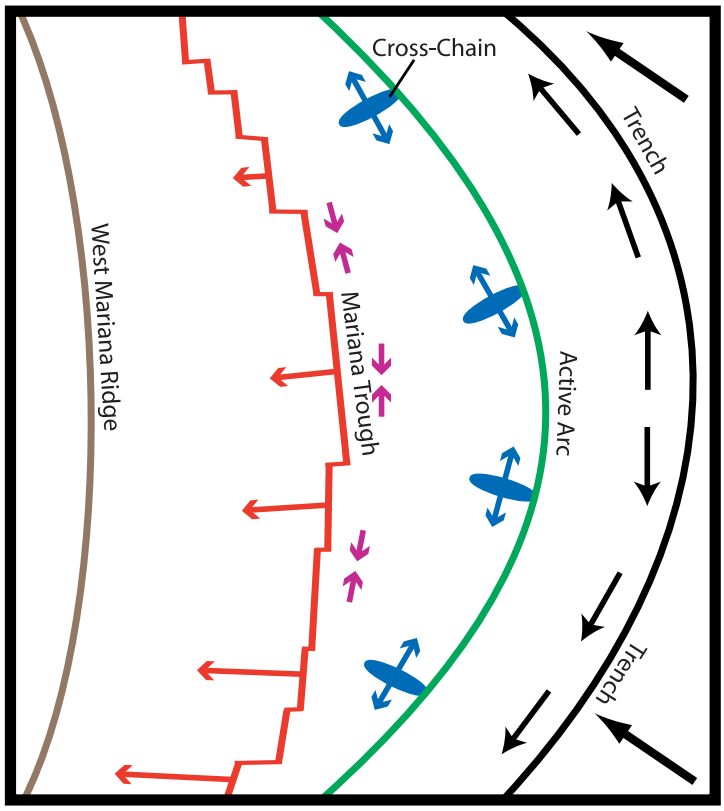

Figure 6. Schematic diagram of arc showing processes causing along-strike extension. Heavy black, green, red and brown lines represent the trench, island arc, back-arc spreading center, and the west Mariana Ridge, respectively. Arc-parallel extension occurs in the fore arc (black arrows) and in the arc (blue arrows) giving rise to cross-arc volcanism (blue ovals); compression (purple arrows) occurs in the back arc where increasing curvature of the arc system induces N–S compression.

complex but consistent with this overall pattern (Figure 6).

6. Conclusions

[24] Seismic observations of several swarms of small earthquakes present strong evidence for significant along-arc extension in the upper plate of the Mariana subduction system between the trench and back-arc spreading center. This extension facilitates the occurrence of volcanic cross chains involving passive mantle upwelling such as those at 14°40′N [*Kohut et al.*, 2006] and the Diamante cross chain. The interaction of different volcanic and tectonic processes likely gives the two cross chains different morphologic and seismic characteristics even though the same overall process is responsible for both. Recent GPS and earthquake slip vector results [*McCaffrey*, 1996; *Bird*, 2003; *Kato et al.*, 2003] also support along arc extension in the southern region though the amount of extension between Saipan and islands further to the north is not yet fully resolved. On the basis of the strong correlation between extensional seismicity and volcanism, it is likely that cross-chain location it tectonically controlled and is centralized in regions with heightened levels of arc-parallel stress and that the style of volcanism is controlled by the presence of active upwelling. While the region around the arc and fore arc is undergoing extension, the back arc region may be undergoing shortening due to the increasing curvature of the arc and the shortening that this creates. The mechanism for the localization of compressional stresses in the back arc does not appear to be as well developed as the mechanism for localizing arc-parallel extension.

Acknowledgments

[25] We thank Bob Stern for helpful comments on an earlier version and numerous people for assistance with deploying and recovering the seismographs, particularly Patrick Shore, Spahr Webb, Allan Sauter, Mitchell Barklage, Brian Shiro, Sara Pozgay, Patrick Jonke, Juan Camacho, Joe Kaipat, and Ray

Chong, as well as the captains and the crews of the R/V *Kaiyo*, the R/V *Wecoma*, and the Super Emerald. Land seismic instrumentation was provided by the PASSCAL program of the Incorporated Research Institutions in Seismology (IRIS) and the Lamont Ocean Bottom Seismograph Facility provided ocean bottom seismographs. This research was supported by the MARGINS program under National Science Foundation grants OCE-0001938 and EAR-0549056. We also thank Bob Stern and Cliff Frolich for helpful reviews.

References

Barker, P. F., and I. W. D. Dalziel (1983), Progress in geodynamics in the Scotia Arc region, in *Geodynamics of the Eastern Pacific Region, Caribbean, and Scotia Arcs*, *Geodyn. Ser.*, vol. 9, edited by R. Cabre, pp. 137–170, AGU, Washington, D. C.

Bird, P. (2003), An updated digital model of plate boundaries, *Geochem. Geophys. Geosyst.*, *4*(3), 1027, doi:10.1029/2001GC000252.

Christensen, N. I. (1996), Poisson's ratio and crustal seismology, *J. Geophys. Res.*, *101*, 3139–3156, doi:10.1029/95JB03446.

Dziewonski, A. M., and D. L. Anderson (1981), Preliminary Earth reference model, *Phys. Earth Planet Inter.*, *25*(4), 297–356, doi:10.1016/0031-9201(81)90046-7.

Embley, R. W., et al. (2006), Long term eruptive activity at a submarine arc volcano, *Nature*, *441*, 494–497, doi:10.1038/nature04762.

Fryer, P. (1996), Evolution of the Mariana convergent plate margin system, *Rev. Geophys.*, *34*(1), 89–125, doi:10.1029/95RG03476.

Fryer, P., J. B. Gill, and M. C. Jackson (1997), Volcanologic and tectonic evolution of the Kasuga seamounts, northern Mariana Trough: *Alvin* submersible investigations, *J. Volcanol. Geotherm. Res.*, *79*, 277–311, doi:10.1016/S0377-0273(97)00013-9.

Gvirtzman, Z., and R. J. Stern (2004), Bathymetry of Mariana trench-arc system and formation of the Challenger Deep as a consequence of weak plate coupling, *Tectonics*, *23*, TC2011, doi:10.1029/2003TC001581.

Hall, R., M. Fuller, J. R. Ali, and C. D. Anderson (1995), The Philippine Sea plate: Magnetism and reconstructions, in *Active Margins and Marginal Basins of the Western Pacific*, *Geophys. Monogr. Ser.*, vol. 88, edited by B. Taylor and J. Natland, pp. 371–404, AGU, Washington, D. C.

Jordan, T. H., and K. A. Sverdrup (1981), Teleseismic location techniques and their application to earthquake clusters in the South-Central Pacific, *Bull. Seismol. Soc. Am.*, *71*(4), 1105–1130.

Kato, T., J. Beavan, T. Matsushima, Y. Kotake, J. T. Camacho, and S. Nakao (2003), Geodetic evidence of back-arc spreading in the Mariana Trough, *Geophys. Res. Lett.*, *30*(12), 1625, doi:10.1029/2002GL016757.

Kennett, B. L. N. (1983), *Seismic Wave Propagation in a Stratified Media*, Cambridge Univ. Press, New York.

Kennett, B. L. N., and E. Engdahl (1991), Traveltimes for global earthquake location and phase identification, *Geophys. J. Int.*, *105*, 429–465, doi:10.1111/j.1365-246X.1991.tb06724.x.

Kohut, E. J., R. J. Stern, A. J. R. Kent, R. L. Nielson, S. H. Bloomer, and M. Leybourne (2006), Evidence for adiabatic decompression melting in the southern Mariana Arc from high-Mg lavas and melt inclusions, *Contrib. Mineral. Petrol.*, *152*, 201–221, doi:10.1007/s00410-006-0102-7.

Kubo, A., and E. Fukuyama (2003), Stress field along the Ryukyu Arc and in the Okinawa Trough inferred from moment tensors of shallow earthquakes, *Earth Planet. Sci. Lett.*, *210*, 305–316, doi:10.1016/S0012-821X(03)00132-8.

Lahr, J. (1999), HYPOELLIPSE: A computer program for determining local earthquake hypocentral parameters, magnitude, and first-motion pattern (y2k compliant version), 1999 version 1.0, U. S. Geol. Surv., Reston, Va.

Langston, C. A., and D. V. Helmberger (1975), A procedure for modeling shallow dislocation sources, *Geophys. J. R. Astron. Soc.*, *42*, 117–130.

Martinez, F., P. Fryer, and N. Beker (2000), Geophysical characteristics of the southern Mariana Trough 11°50′N–13°40′N, *J. Geophys. Res.*, *105*(B7), 16,591–16,607, doi:10.1029/2000JB900117.

McCaffrey, R. (1996), Estimates of modern arc parallel strain rates in fore-arcs, *Geology*, *24*(1), 27–30, doi:10.1130/0091-7613(1996)024<0027:EOMAPS>2.3.CO;2.

Miller, M. S., A. Gorbatov, and B. L. N. Kennett (2006), Three-dimensional visualization of a near-vertical slab tear beneath the southern Mariana Arc, *Geochem. Geophys. Geosyst.*, *7*, Q06012, doi:10.1029/2005GC001110.

Pavlis, G. L., F. Vernon, D. Harvey, and D. Quinlan (2004), The generalized earthquake-location (GENLOC) package: And earthquake-location library, *Comput. Geosci.*, *30*, 1079–1091, doi:10.1016/j.cageo.2004.06.010.

Pozgay, S. H., R. A. White, D. A. Wiens, P. J. Shore, A. W. Sauter, and J. L. Kaipat (2005), Seismicity and tilt associated with the 2003 Anatahan eruption sequence, *J. Volcanol. Geotherm. Res.*, *146*(1–3), 60–76, doi:10.1016/j.jvolgeores.2004.12.008.

Pozgay, S. H., D. A. Wiens, J. A. Conder, H. Shiobara, and H. Sugioka (2007), Complex mantle flow in the Mariana subduction system: Evidence from shear wave splitting, *Geophys. J. Int.*, *170*(1), 371–386, doi:10.1111/j.1365-246X.2007.03433.x.

Quinlan, D. M., D. Harvey, and G. Wagner (1996), Datascope seismic application package, *Seismol. Res. Lett.*, *67*(2), 51.

Schellart, W. P. (2005), Influence of the subducting plate velocity on the geometry of the slab and migration of the subduction hinge, *Earth Planet. Sci. Lett.*, *231*, 197–219, doi:10.1016/j.epsl.2004.12.019.

Schellart, W. P., J. Freeman, D. R. Stegman, L. Moresi, and D. May (2007), Evolution and diversity of subduction zones controlled by slab width, *Nature*, *446*, 308–311, doi:10.1038/nature05615.

Shaw, P. R. (1994), Age variations of oceanic crust Poisson's ration: Inversion and a porosity evolution model, *J. Geophys. Res.*, *99*(B2), 3057–3066, doi:10.1029/93JB02109.

Stern, R. J., and N. C. Smoot (1998), A bathymetric overview of the Mariana forearc, *Isl. Arc*, *7*, 525–540, doi:10.1111/j.1440-1738.1998.00208.x.

Stern, R. J., M. C. Jackson, P. Fryer, and E. Ito (1993), O, Sr, Nd, and Pb isotopic composition of the Kasuga cross-chain in the Mariana Arc: A new perspective on the K-h relationships, *Earth Planet. Sci. Lett.*, *119*, 459–476, doi:10.1016/0012-821X(93)90056-F.

Stern, R. J., M. J. Fouch, and S. L. Klemperer (2003), An overview of the Izu-Bonin Mariana subduction factory, in *Inside the Subduction Factory*, *Geophys. Monogr. Ser.*, vol. 138, edited by J. M. Eiler, pp. 175–222, AGU, Washington, D. C.

Stern, R. J., E. Kohut, S. H. Bloomer, M. Leybourne, M. Fouch, and J. Vervoot (2006), Subduction factory processes beneath the Guguan cross-chain, Mariana Arc: No role for sediments, are serpentinites important?, *Contrib. Mineral. Petrol.*, *151*, 202–221, doi:10.1007/s00410-005-0055-2.

Takahashi, N., S. Kodaira, S. L. Klemperer, Y. Tatsumi, Y. Kaneda, and K. Suyehiro (2007), Crustal structure and evolution of the Mariana intra-oceanic island arc, *Geology*, *35*(3), 203–206, doi:10.1130/G23212A.1.

Webb, S. C., T. K. Deaton, and J. C. Lemire (2001), A broadband ocean-bottom seismometer based on a 1-Hz natural period geophone, *Bull. Seismol. Soc. Am.*, *91*(2), 304–312, doi:10.1785/0120000110.